Journal of Power Sources 196 (2011) 5797–5802

Contents lists available at ScienceDirect

Journal of Power Sources

journal homepage: www.elsevier.com/locate/jpowsour

Stability and performance of infiltrated $La_{0.8}Sr_{0.2}Co_xFe_{1-x}O_3$ electrodes with and without $Sm_{0.2}Ce_{0.8}O_{1.9}$ interlayers

L. Adijanto, R. Küngas, F. Bidrawn, R.J. Gorte, J.M. Vohs*

Department of Chemical and Biomolecular Engineering, University of Pennsylvania, Philadelphia, PA 19104, USA

ARTICLE INFO

Article history:
Received 5 February 2011
Received in revised form 8 March 2011
Accepted 9 March 2011
Available online 21 March 2011

Keywords:
Solid oxide fuel cells
Cathode deactivation
Yttria-stabilized zirconia
Lanthanum strontium cobalt ferrite
Ceria

ABSTRACT

The chemical stability of composite electrodes produced by the infiltration of $La_{0.8}Sr_{0.2}Co_xFe_{1-x}O_3$ (LSCF) into a porous yttria-stabilized zirconia (YSZ) scaffold were investigated as a function of the Co:Fe ratio in the LSCF and the LSCF calcination temperature. XRD and impedance spectroscopy results indicate that for an LSCF calcination temperature of 1123 K, reactions between the LSCF and YSZ do not occur to a significant extent. Reactions producing $La_2Zr_2O_7$ and $SrZrO_3$ at the interface were observed, however, for a calcination temperature of 1373 K and x values greater than 0.2. In addition to determining the conditions for which reactions between LSCF and YSZ occur, the effectiveness of infiltrated SDC interlayers in preventing reactions at the LSCF–YSZ interface and their influence on the overall performance of LSCF/YSZ composite electrodes was studied.

1. Introduction

The most commonly used cathode in solid oxide fuel cells (SOFCs) consists of a porous composite of electronically conducting Sr-doped lanthanum manganite (LSM) and the electrolyte, yttria-stabilized zirconia (YSZ). While the performance of these cathodes is acceptable at temperatures above 1073 K, their electrochemical performance is marginal at lower temperatures due to the relatively low electronic conductivity of the LSM. The push to lower the operating temperature of SOFC has, therefore, also motivated the development of cathodes with higher performance at lower temperatures. Using mixed conducting (i.e. electronic and ionic) perovskites such as Sr-doped lanthanum ferrite ($La_{0.8}Sr_{0.2}FeO_3$, LSF) [1–6] and Sr-doped lanthanum cobaltite ($La_{0.8}Sr_{0.2}CoO_3$, LSC) [7–11] is one approach that is being used to enhance cathode performance at intermediate temperatures (873–973 K). The ionic conductivity in these materials allows O^{2-} ions to be transported through the perovskite to the YSZ thereby providing more active surface area. LSC has relatively high electronic conductivity at (1220 S cm^{-1} at 800 °C [12]) and good oxygen exchange characteristics [13–16] making it particularly attractive for cathode applications. Unfortunately LSC reacts with YSZ at temperatures above 1273 K [17] forming non-conducting phases at the LSC–YSZ interface; thus, low-temperature electrode synthesis procedures are required in order to fabricate LSC/YSZ composite cathodes. When such approaches are used (e.g. sol–gel [18] or wet infiltration [19–24]) LSC–YSZ cathodes exhibit excellent initial performance at 973 K, but rapid degradation due to reaction at the interface still occurs [10].

LSF appears to be more chemically compatible with YSZ and the reactions between these materials producing new phases only becomes evident via XRD at temperatures above 1673 K [10,19,25–27]. It has been suggested that a small amount of Zr^{4+} may become incorporated into the B site of LSF at the LSF–YSZ interface and this may affect properties [4,26], but changes in the LSF lattice parameter which would signify this type of substitution have only been observed at temperatures higher than those used in the preparation of the LSF–YSZ electrodes [19]. Additionally, it has been reported that a $La_{0.8}Sr_{0.2}Fe_{0.9}Zr_{0.1}O_3$ cathode exhibits performance similar to LSF [19]. While reactions between LSF and YSZ do not appear to be problematic, the performance of LSF–YSZ cathodes is limited by their lower electronic conductivity relative to LSC [28]. As a compromise between LSC and LSF, solid solutions of these materials ($La_{1-y}Sr_yCo_xFe_{1-x}O_3$, LSCF) are often used, and LSCF–YSZ composite cathodes have been reported to exhibit excellent performance [29–31].

Thin interlayers of ionically conducting ceria doped with samaria (SDC) or gadolinia (GDC) are often used to separate LSF or LSC from YSZ in order to enhance cathode performance [3,4,32]. For LSC, the ceria interlayer prevents reaction with the YSZ both during fabrication and cell operation. The effect of ceria interlayers on the performance of LSF and LSCF cathodes is less clear. While prevent-

* Corresponding author at: Chemical Engineering, University of Pennsylvania, 220 S. 33rd Street, Philadelphia, PA 19104-6393, USA. Tel.: +1 215 898 6318; fax: +1 215 573 2093.
E-mail address: vohs@seas.upenn.edu (J.M. Vohs).

0378-7753/$ – see front matter © 2011 Elsevier B.V. All rights reserved.
doi:10.1016/j.jpowsour.2011.03.022

ing reactions with the YSZ is often used as justification for the need for a ceria interlayer when using LSF, as noted above, reaction of LSF with the YSZ does not appear to occur for typical SOFC fabrication conditions. Nonetheless, it has been reported that SDC interlayers still significantly enhance the performance of LSF cathodes [4,32]. Simner et al. have suggested that the improved performance is a consequence of the higher ionic conductivity and surface reaction exchange kinetics of SDC relative to YSZ [4]. While ceria interlayers are also generally used for LSCF cathodes, the mechanism by which the interlayer affects performance is again not well understood. Preventing Co from reacting with the YSZ is one potential role, but the conditions at which such reactions may occur for LSCF and the effect of the Co to Fe ratio have yet to be determined.

Infiltration in which the constituent ions in the perovskite phase (e.g. LSF, LSCF) of the cathode are added to a YSZ porous electrode scaffold in the form of aqueous solutions and then calcined in air to form the desired phase has become a popular method for cathode synthesis [19–24]. This approach has the advantage of significantly reducing the sintering temperature required when adding the perovskite phase, which in some cases, such as LSC, allows reactions with the YSZ to be avoided. This synthesis method also produces a unique structure in which the active component coats the YSZ rather than forming a random composite of the two materials. Issues relating to mismatches in the coefficients of thermal expansion (CTE) of the two materials are also often avoided using the infiltration method. We have recently shown that doped-ceria interlayers can be incorporated into cathodes using infiltration [17]. In this work it was shown that wet infiltration of the constituent ions in SDC followed by calcination at 1123 K produces a porous coating of SDC nanoparticles over the YSZ. This porous layer, however, can be transformed into a dense coating by calcination at 1473 K. Infiltrated, dense SDC coatings were found to prevent reaction between LSC (also added by infiltration) and YSZ for calcination temperatures up to 1373 K and LSC/SDC/YSZ electrodes produced in this manner were found to exhibit excellent performance with an ASR of 20–30 $m\Omega\,cm^2$ at 973 K.

The use of infiltration techniques for cathode synthesis when comparing the performance of electrodes with different compositions has the benefit that electrodes with very similar structures can be produced for a range of compositions, thereby eliminating large structural variations as one possible cause for performance variations. In the present study we have used infiltration to produce $La_{1-y}Sr_yCo_xFe_{1-x}O_3$ ($0 \le x \le 1$)–YSZ composite electrodes both with and without SDC interlayers and have investigated the range of compositions of LSCF for which the formation of new phases via reaction with YSZ does not occur for typical SOFC fabrication and operating temperatures. We have also studied how SDC interlayers affect the performance of LSF and LSCF cathodes with the goal of determining whether preventing reactions at the LSF– and LSCF–YSZ interfaces plays a significant role in enhancing cathode performance.

2. Experimental

The fuel cells used in this study were fabricated using porous-dense-porous YSZ scaffolds that were produced via sintering laminated green YSZ (Tosoh Corp., 8 mol% Y_2O_3-doped ZrO_2, 0.2 μm) tapes as described in detail elsewhere [33]. The tapes that were used to produce the porous layers contained graphite as a sacrificial pore former in addition to YSZ. For each cell, the dense electrolyte layer was 100 ± 5 μm in thickness and 1 cm in diameter. The two porous layers, which were used for the electrodes, were each 50 ± 2 μm in thickness and 0.67 cm in diameter. They were also ~65% porous with a BET surface area 0.3 $m^2\,g^{-1}$. LSF, LSC, and LSCF cathodes were prepared using the infiltration method developed in our lab [6,10,19,20]. Aqueous solutions of $La(NO_3)_3{\cdot}6H_2O$ (Alfa Aesar, 99.9%), $Sr(NO_3)_2$ (Alfa Aesar, 99%), $Co(NO_3){\cdot}6H_2O$ (Aldrich, 99%) and $Fe(NO_3)_3{\cdot}9H_2O$ (Fisher Scientific) were used as the precursor solutions. Citric acid (Fisher Scientific) was added, in a 1:1 ratio for each cation, as a complexing agent to allow formation of the perovskite phase at a lower temperature. Multiple infiltration steps were required to reach the desired 40 wt% loading of perovskite and the samples were calcined to 723 K after each infiltration. After reaching the desired loading, the samples were calcined to either 1123 K or 1373 K for 4 h. Cells were fabricated for the following perovskite compositions: $La_{0.8}Sr_{0.2}FeO_3$ (LSF), $La_{0.8}Sr_{0.2}CoO_3$ (LSC) and $La_{0.8}Sr_{0.2}Co_xFe_{1-x}O_3$ (LSCF) with $0 \le x \le 1.0$ (LSC20F for $x = 0.2$, LSC40F for $x = 0.4$, etc.).

Cells were also fabricated in which $Sm_{0.2}Ce_{0.8}O_{1.9}$ (SDC) was used as an interlayer between the perovskite and the YSZ. The SDC interlayer was prepared using multiple infiltration steps with an aqueous mixture of $Ce(NO_3)_3{\cdot}6H_2O$ (Alfa Aesar, 99.5%) and $Sm(NO_3)_3{\cdot}6H_2O$ (Alfa Aesar, 99.9%) followed by heating in air to 723 K. After sufficient SDC had been added to produce a dense coating ~0.1 μm in thickness over the YSZ, the cell was calcined in air at 1473 K for 4 h. As we have reported previously, this annealing treatment produces a dense, continuous SDC coating over the YSZ [17]. After fabricating the SDC interlayer, LSF, LSC, or LSCF were added using the infiltration procedure described above.

After preparing the cathodes, 50 wt% CeO_2 and 0.5 wt% Pd was added to the porous YSZ layer on the other side of the cell using a similar infiltration procedure to produce the anode. Silver paste was used as the current collector for both the anode and cathode and the cells were mounted onto an alumina tube with a ceramic adhesive (Aremco, Ceramabond 552). All cell testing was performed with the anode exposed to humidified H_2 (3% H_2O) and the cathode to ambient air. X-ray diffraction (XRD) using Cu Kα radiation was used to determine the phases present in the LSCF–YSZ cathode. Electrochemical impedance spectroscopy (Gamry Instruments) and V-I polarization curves were used to characterize the performance of each cathode formulation. The impedance spectra were measured galvanostatically at various currents in the frequency range of 300 kHz to 0.01 Hz, with a 1 mA AC perturbation.

3. Results and discussion

3.1. XRD results

XRD was used to investigate the reaction of LSCF with YSZ as a function of the ratio of the B-site cations and temperature. XRD patterns of 40 wt% LSCF–YSZ composites which had been calcined at 1123 K for 4 h are shown in Fig. 1 for x values between 0 and 1. The peaks at 30° and 35° correspond to the fluorite lattice of the YSZ substrate. The peak at 32.1° in the spectrum of LSF is indicative of the orthorhombic structure of this material [34,35]. The position of this peak shifts to higher values upon the incorporation of Co into the lattice and appears at 32.5° for a Co:Fe ratio of 4:6 (i.e. LSC40F). Some broadening of the peak is also evident at this Co:Fe ratio. Since pure LSC has a rhombohedral structure [17,36] for which this peak splits into two peaks, the observed broadening with Co addition is likely due to this phase transformation. For higher Co:Fe ratios, the peaks indicative of the rhombohedral distortion of the perovskite structure remain fixed at 33.0°. A slight shift to 33.2° is observed for the pure LSC. Even for the LSC it was not possible to resolve the two separate components of this peak. This is likely due to the presence of relatively small crystallites in the 1123 K annealed samples resulting in significant line broadening. An important aspect of the XRD data in Fig. 1 is that there is no evidence for the formation of secondary phases, such as $La_2Zr_2O_7$ or $SrZrO_3$, which would result from the reaction of the LSCF with the YSZ.

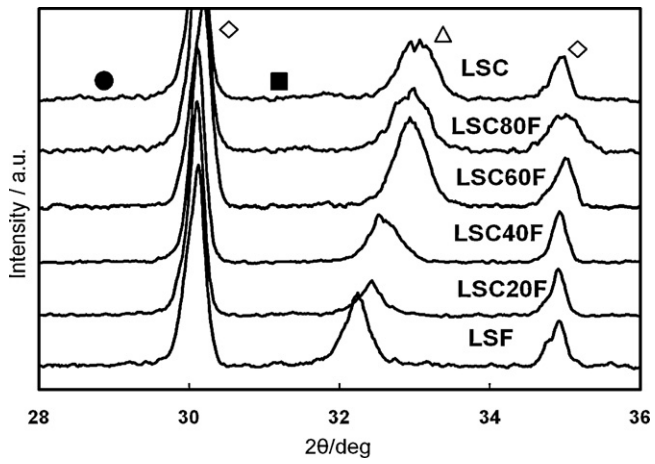

Fig. 1. XRD patterns of $La_{0.8}Sr_{0.2}Co_xFe_{1-x}O_3$ -YSZ composites that had been calcined to 1123 K with the indicated compositions. The peak positions correspond to: (●) $La_2Zr_2O_7$, (■) $SrZrO_3$, (◊) YSZ, and (Δ) $La_{0.8}Sr_{0.2}Co_xFe_{1-x}O_3$.

An analogous set of XRD data for a 40 wt% LSCF–YSZ composites, which had been calcined at 1373 K for 4 h, are shown in Fig. 2. The patterns for the LSF–YSZ and LSC20F–YSZ samples are essentially identical to those of the corresponding samples calcined at only 1123 K, except the peaks are narrower indicating a larger crystallite size. Thus for these compositions, the XRD data indicates that LSCF does not react with YSZ for temperatures up to 1373 K. This result is consistent with previous studies that have also shown that LSF does not react with YSZ for calcination temperatures up to 1473 K [4,37]. For larger values of x, however, the XRD results clearly show reaction at the LSCF–YSZ interface occurs. For $x \geq 0.4$ new peaks emerge at 28.5° and 33.5° which correspond to lanthanum zirconate, $La_2Zr_2O_7$. Additionally for $x \geq 0.6$, a small peak at 30.9° is evident which corresponds to strontium zirconate, $SrZrO_3$. The remaining peaks in these patterns, i.e. the doublet between 32.5° and 34°, correspond to LSCF. The positions of these peaks increase with increasing Co:Fe ratio, consistent with what was observed for the samples calcined at 1123 K. The fact that the doublet is now resolved also indicates a larger average crystallite size in the LSCF film in the samples calcined at 1373 K relative to those calcined at only 1123 K.

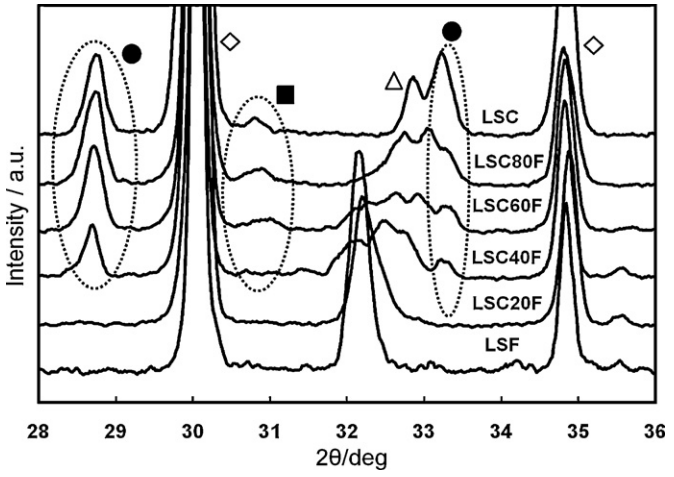

Fig. 2. XRD patterns of $La_{0.8}Sr_{0.2}Co_xFe_{1-x}O_3$ -YSZ composites that had been calcined to 1373 K with the indicated compositions. The peak positions correspond to: (●) $La_2Zr_2O_7$, (■) $SrZrO_3$, (◊) YSZ, and (Δ) $La_{0.8}Sr_{0.2}Co_xFe_{1-x}O_3$.

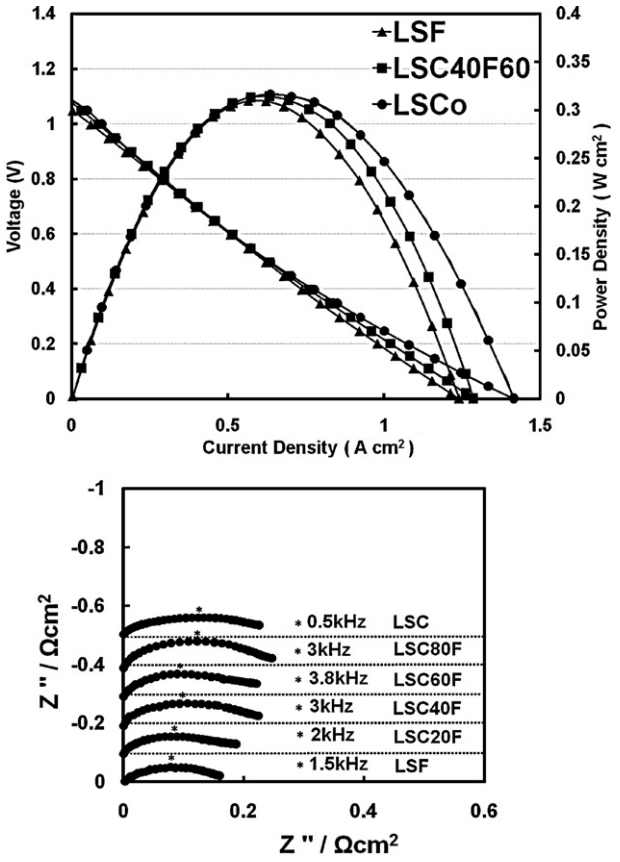

Fig. 3. Polarization curves electrochemical impedance spectra obtained at open circuit for fuel cells with infiltrated LSCF cathodes that had been calcined at 1123 K. The composition of the LSCF used in each cell is indicated in figure.

3.2. Effect of cobalt concentration

Fig. 3 displays Nyquist plots of the open-circuit electrochemical impedance data at 973 K for all of the LSCF–YSZ composites that were sintered at 1123 K. Polarization curves for a subset of the LSCF–YSZ compositions are also shown in the figure. The ohmic impedances of the cells varied by less than 0.1 Ω cm² and have been subtracted from the spectra to facilitate comparison. LSC has a higher electronic and ionic conductivity than LSF and increasing the Co to Fe ratio in the perovskite would therefore be expected to extend the width of the active TPB region and give higher performance [1,12,19,20,30,31]. As shown in figure, this is not what was observed and instead the ASR of the electrodes increased from 0.18 Ω cm² for LSF to 0.22 and 0.21 Ω cm² for LSC80F and LSC, respectively. The XRD results in Fig. 1 do not provide evidence for reaction between LSC or LSCF and YSZ for a calcination temperature of only 1173 K, but the impedance results suggest that some reaction at the interface may still occur for these conditions. The possibility that slight structural variations are the origin of the small differences can also not be completely ruled out.

The open-circuit impedance spectra at 973 K for LSCF–YSZ composites that were calcined at 1373 K are shown in Fig. 4. Polarization curves for a subset of the LSCF–YSZ compositions are also shown in figure. Declines in performance were observed and the ASR of the electrodes all increased for this higher calcination temperature. The increases were much more precipitous, however, for the higher cobalt content electrodes. For example, the ASR of the LSF– and LSC20F–YSZ composite electrodes increased by ~1.2 Ω cm² upon increasing the calcination temperature from 1173 to 1373 K. In contrast for LSC60F, LSC80F and LSC, the ASR increased by 7.6, 8.5,

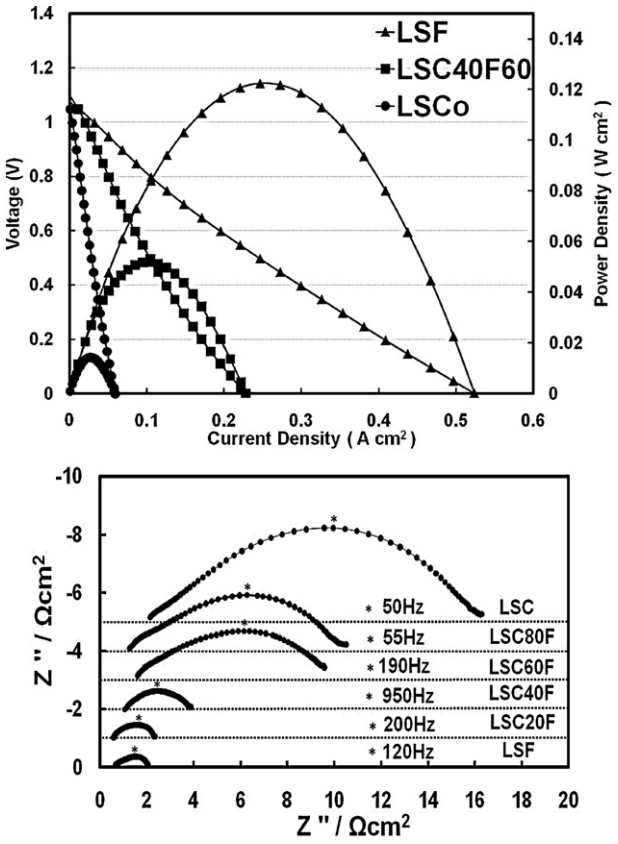

Fig. 4. Polarization curves and electrochemical impedance spectra obtained at open circuit for fuel cells with infiltrated LSCF cathodes that had been calcined at 1373 K. The composition of the LSCF used in each cell is indicated in figure.

and 13.7 $\Omega\,cm^2$, respectively. We have previously shown that significant coarsening of the LSCF particles occurs upon calcination at 1373 K [28]. This causes a decrease in TPB sites and is likely the cause of the increase in the ASR for the LSF- and LSC20F-YSZ composites. The large increases for high Co:Fe ratios, however, are almost certainly due to reaction of the LSCF and the YSZ forming insulating $La_2Zr_2O_7$ or $SrZrO_3$ phases at the interface as demonstrated by the XRD results in Fig. 2.

The data in Fig. 4 also show that the ohmic resistance of the cells increased with increasing Co content in the perovskite. This occurred in spite of the fact that increasing the Co content increases the electronic conductivity of the LSCF and provides additional evidence for the formation of insulating phases at the LSCF–YSZ interface. The data also show, however, that the propensity for the LSCF to react with the YSZ to form $La_2Zr_2O_7$ or $SrZrO_3$ is a strong function of the Co:Fe ratio in the perovskite. Note that formation of these insulating phases is much less problematic for Co concentrations less than 40%. Indeed the ASR of LSC20F is nearly identical to that of LSF, even after calcining at 1373 K. This suggests that the LSC20F composition may provide a good compromise between the increase in electronic conductivity and the decrease in chemical stability that added Co imparts to LSF.

3.3. Effectiveness of SDC interlayers

As noted above, thin ceria layers between the YSZ and the perovskite phase are often used to enhance or stabilize cathode performance. For some cathode materials such as LSC, ceria interlayers clearly act as a protective barrier that prevents reactions at the LSC–YSZ interface [13,17,38,39]. Even for cathode materials, such as LSF, which do not appear to react with YSZ under typical synthesis and operating conditions, there are reports in the literature that ceria interlayers still enhance performance [4,32]. In this case, the mechanism by which the ceria could enhance performance is less clear, although increasing the active surface area and improving the O_2 surface exchange kinetics [4,22,32] have both been proposed. To further investigate these possibilities we investigated the effect of an SDC interlayer prepared using infiltration methods on the performance and stability of LSF-, LSC20F-, and LSC-YSZ composite cathodes.

SDC layers, approximately 0.1 μm in thickness, were added to the porous YSZ scaffolds using wet infiltration as described in Section 2 and were calcined at 1473 K for 2 h prior to adding the perovskite phase and then calcined at 1373 K for 4 h. We have previously shown that the 1473 K calcination treatment for the SDC layer produces a continuous, dense SDC coating over the YSZ [17,40]. Fig. 5 shows electrochemical impedance spectra for the LSF-, LSC20F-, and LSC-based electrodes, both with and without the SDC interlayer, at 973 K. Note that for the LSF and LSC20F cathodes the addition of the SDC interlayer had a negligible effect on the impedance characteristics and thermal stability. The ohmic and non-ohmic ASR for both LSF and LSC20F calcined at 1373 K were $0.57 \pm 0.1\ \Omega\,cm^2$ and $1.5 \pm 0.1\ \Omega\,cm^2$, respectively, with or without the SDC layer. These results are consistent with the XRD data in Fig. 2 which shows that these materials do not react with YSZ at temperatures up to 1373 K.

As shown by a comparison of the data in Figs. 3 and 5, the performance of the infiltrated LSF and LSC20F electrodes, with or without SDC interlayers, still degraded upon increasing the calcination temperature of the perovskite phase from 1123 to 1373 K. As we have reported previously for LSF–YSZ electrodes [19], we believe that this degradation results from additional coarsening of the LSF and LSC20F particles at the higher calcination temperature resulting in a loss of active surface area and the formation of a more dense coating of the perovskite phase over the YSZ. This decreases the concentration of exposed TPB sites and increases the average distance that the oxygen ions must travel through the LSCF. A decrease in the performance of screen-printed LSCF electrodes upon increasing the calcination temperature form 1353 to 1393 K has also been partly attributed to a loss in surface area by Mai et al. [37].

Our observation that SDC interlayers do not affect the performance and stability of infiltrated LSF and LSC20F electrodes is different than what has been reported in previous studies of screen printed electrodes in which positive effects for ceria interlayers have been observed [4,26,32]. For example, Simner et al. [4] report significant performance enhancements when a several micron thick porous SDC layer is placed between the LSF and the dense YSZ electrolyte. Mai et al. report similar results for LSC20F using gadolinia-doped ceria (GDC) [37] interlayers. In both of these studies it is suggested that the improvement in performance is at least partially due to the high ionic conductivity of the doped ceria, which presumably increases the density of active TPB sites. Mai et al. also suggest that for LSC20F that contains a high ratio of Sr to La, preventing the formation of $SrZrO_3$ via reaction with the YSZ still plays a role.

The suggestion that ceria interlayers enhance performance via increasing ionic conductivity may indeed be the case when conventional methods are used for cathode fabrication, such as screen printing a slurry containing particles of the perovskite onto an already dense YSZ electrolyte layer, followed by calcination in air. In this approach the calcination temperature, must be low enough to prevent reaction between the perovskite and the YSZ and is typically between 1423 K and 1523 K, which may be too low to form a well sintered, interconnected perovskite phase in the electrode. For electrodes formed in this manner there may be relatively few channels for oxygen ion transport in the mixed

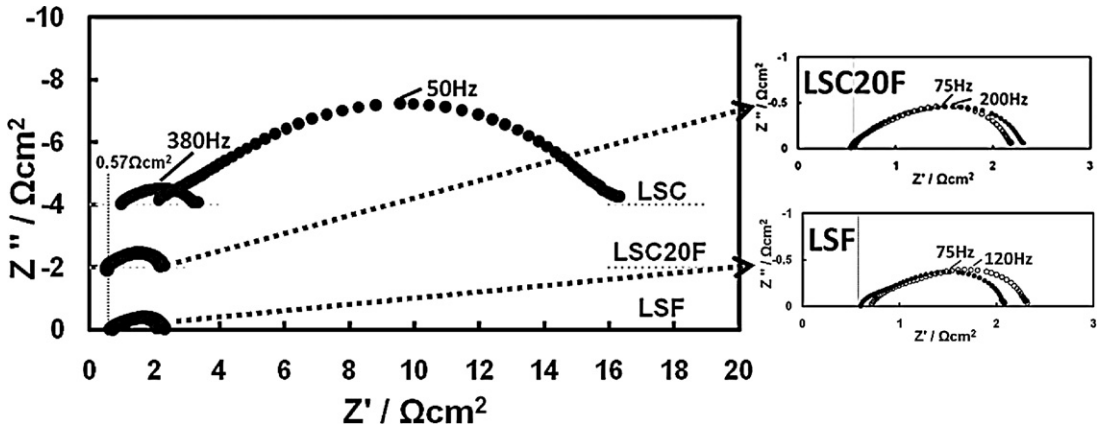

Fig. 5. Electrochemical impedance spectra obtained at open circuit for fuel cells with infiltrated LSC, LSC20F, and LSF cathodes with (open symbols) and without (filled symbols) infiltrated SDC interlayers. The cathodes were calcined at 1373 K prior to colleting the data.

conducting perovskite. This will limit the thickness of the active TPB region and degrade overall performance. For electrodes with this structure, a porous SDC interlayer may help to enhance O^{2-} ion transport and produce electrodes with thicker electrochemically active regions. The situation is different, however, for the infiltrated cathodes used in this study where the electrode architecture consists of a thin film of the perovskite covering a highly porous, well sintered, YSZ or SDC-coated YSZ backbone, both of which provide channels for ion conduction and therefore large TPB regions.

In contrast to LSF and LSC20F, the addition of an SDC interlayer had a dramatic effect on the performance and stability of the LSC–YSZ composite electrode. Without the SDC layer the ohmic and non-ohmic ASR were 2.1 $\Omega\,cm^2$ and 14 $\Omega\,cm^2$, respectively. Note that the non-ohmic ASR is 1.5 $\Omega\,cm^2$, greater than the expected value for the 100 μm thick YSZ electrolyte. As shown by the XRD data in Fig. 2, the high ohmic and non-ohmic ASR are clearly due to reaction at the LSC–YSZ interface resulting in the formation of insulting layers of $La_2Zr_2O_7$ and $SrZrO_3$. Placing an SDC layer between the LSC and YSZ was effective in preventing these deleterious reactions from taking place although modest increases in the ohmic and non-ohmic ASR to 0.97 $\Omega\,cm^2$ and 2.1 $\Omega\,cm^2$, respectively, were still observed.

4. Conclusions

The propensity of infiltrated layers of $La_{0.8}Sr_{0.2}Co_xFe_{1-x}O_3$ to react with YSZ was studied as a function of the LSCF calcination temperature and the Co:Fe ratio. For a calcination temperature of 1123 K, both XRD and impedance spectroscopy did not provide any evidence for significant reaction at the LSCF–YSZ interface for all LSCF compositions. For a calcination temperature of 1373 K, however, reaction at the interface to form insulating $La_2Zr_2O_7$ and $SrZrO_3$ phases was observed for x values greater than 0.2. This result suggests that LSC20F may provide a good compromise between the higher electronic conductivity and lower chemical compatibility with YSZ that occurs with increasing Co concentration in the LSCF.

Infiltrated SDC interlayers were also shown to be effective in preventing deleterious, solid-state, reactions at the LSCF–YSZ interface. In contrast to previous studies of LSCF electrodes with doped-ceria interlayers that were produced by screen printing, infiltrated SDC interlayers covering a porous YSZ electrode scaffold were not found to provide any enhancement of the overall performance of LSF or LSC20F.

Acknowledgement

This work was funded by the U.S. Department of Energy's Hydrogen Fuel Initiative (grant DE-FG02-05ER15721).

References

[1] H. Kishimoto, N. Sakai, T. Horita, K. Yamaji, M.E. Brito, H. Yokokawa, Solid State Ionics 178 (2007) 1317.
[2] J.M. Ralph, C. Rossignol, R. Kumar, J. Electrochem. Soc. 150 (2003) A1518.
[3] S.P. Simner, J.F. Bonnett, N.L. Canfield, K.D. Meinhardt, V.L. Sprenkle, J.W. Stevenson, Electrochem. Solid State Lett. 5 (2002) A173.
[4] S.P. Simner, J.F. Bonnett, N.L. Canfield, K.D. Meinhardt, J.P. Shelton, V.L. Sprenkle, J.W. Stevenson, J. Power Sources 113 (2003) 1.
[5] S.P. Simner, M.D. Anderson, J.W. Stevenson, J. Am. Ceram. Soc. 87 (2004) 1471.
[6] Y. Huang, J.M. Vohs, R.J. Gorte, J. Electrochem. Soc. 151 (2004) A646.
[7] H. Uchida, S. Arisaka, M. Watanabe, Solid State Ionics 135 (2000) 347.
[8] T. Horita, K. Yamaji, N. Sakai, H. Yokokawa, A. Weber, E. Ivers-Tiffee, Electrochim. Acta 46 (2001) 1837.
[9] S.J. Skinner, Int. J. Inorg. Mater. 3 (2001) 113.
[10] Y. Huang, K. Ahn, J.M. Vohs, R.J. Gorte, J. Electrochem. Soc. 151 (2004) A1592.
[11] R. Küngas, I. Kivi, K. Lust, G. Nurk, E. Lust, J. Electroanal. Chem. 629 (2009) 94.
[12] C. Sun, R. Hui, J. Roller, J. Solid State Electrochem. 14 (2010) 1125.
[13] M. Shiono, K. Kobayashi, T.L. Nguyen, K. Hosoda, T. Kato, K. Ota, M. Dokiya, Solid State Ionics 170 (2004) 1.
[14] J. Mizusaki, J. Tabuchi, T. Matsuura, S. Yamauchi, K. Fueki, J. Electrochem. Soc. 136 (1989) 2082.
[15] Y. Teraoka, H.M. Zhang, K. Okamoto, N. Yamazoe, Mater. Res. Bull. 23 (1988) 51.
[16] S. Sekido, H. Tachibana, Y. Yamamura, T. Kambara, Solid State Ionics 37 (1990) 253.
[17] R. Küngas, F. Bidrawn, J.M. Vohs, R.J. Gorte, Electrochem. Solid State Lett. 13 (2010) B87.
[18] C. Peters, A. Weber, E. Ivers-Tiffèe, J. Electrochem. Soc. 155 (2008) B730.
[19] W. Wang, M.D. Gross, J.M. Vohs, R.J. Gorte, J. Electrochem. Soc. 154 (2007) B439.
[20] J.M. Vohs, R.J. Gorte, Adv. Mater. 21 (2009) 943.
[21] S.P. Jiang, J. Mater. Sci. A 418 (2006) 199.
[22] T.Z. Sholklapper, C. Lu, C.P. Jacobson, S.J. Visco, L.C. De Jonghe, Electrochem. Solid State Lett. 9 (2006) A376.
[23] M. Shah, S.A. Barnett, Solid State Ionics 179 (2008) 35.
[24] K.K. Hansen, M. Wandel, Y.-L. Liu, M. Mogensen, Electrochim. Acta 55 (2010) 4606.
[25] J. Hole, D. Kuseer, M. Hrovat, S. Bernik, D. Kolar, Solid State Ionics 95 (1997) 259.
[26] S.P. Simner, J.P. Shelton, M.D. Anderson, J.W. Stevenson, Solid State Ionics 161 (2003) 11.
[27] S.P. Simner, J.F. Bonnett, N.L. Canfield, K.D. Meinhardt, J.P. Shelton, V.L. Sprenkle, J.W. Stevenson, Proceedings of the 2002 Fuel Cell Seminar, Palm Springs, CA, 2002, p. 344.
[28] F. Bidrawn, G. Kim, N. Aramrueang, J.M. Vohs, R.J. Gorte, J. Power Sources 195 (2010) 720.
[29] S.P. Jiang, Solid State Ionics 146 (2002) 1.
[30] A. Esquirol, N.P. Brandon, J.A. Kilner, M. Mogensen, J. Electrochem. Soc. 151 (2004) A1847.
[31] J.H. Kim, Y.M. Park, H. Kim, J. Power Sources 196 (2011) 3544.
[32] A. Martínez-Amesti, A. Larrãnaga, L.M. Rodríguez-Martínez, A.T. Aguayo, J.L. Pizarro, M.L. Nó, A. Laresgoiti, M.I. Arriortua, J. Power Sources 185 (2008) 401.

[33] S. Park, R.J. Gorte, J.M. Vohs, J. Electrochem. Soc. 148 (2001) A443.
[34] N. Orlovskaya, H. Anderson, M. Brodnikovskyy, M. Lugovy, M.J. Reece, J. Appl. Phys. 100 (2006) 026102.
[35] S.E. Dann, D.B. Currie, M.T. Weller, M.F. Thomas, A.D. Al-Rawwas, J. Solid State Chem. 109 (1994) 134.
[36] Y. Jiang, F. Bridges, N. Sundaram, D.P. Belanger, I.E. Anderson, J.F. Mitchell, H. Zheng, Phys. Rev. B 80 (2009) 144423.
[37] A. Mai, V.A.C. Haanappel, S. Uhlenbruck, F. Tietz, D. Stöver, Solid State Ionics 176 (2005) 1341.
[38] M. Sase, D. Ueno, K. Yashiro, A. Kaimai, T. Kawada, J. Mizusaki, J. Phys. Chem. Solids 66 (2005) 343.
[39] C. Rossignol, J.M. Ralph, J.-M. Bae, J.T. Vaughey, Solid State Ionics 175 (2004) 59.
[40] G. Kim, J.M. Vohs, R.J. Gorte, J. Mater. Chem. 18 (2008) 2386.